

BIOCHE 01655

Solvent damping of internal processes in myoglobin studied by specific heat spectroscopy and flash photolysis

M. Settles, F. Post, D. Müller, A. Schulte¹ and W. Doster

Technische Universität München, Physik-Department E13, D-8046 Garching (FRG)

(Received 3 July 1991; accepted in revised form 18 December 1991)

Abstract

We address the question of dynamic coupling between protein and solvent by comparing the enthalpy relaxation of the solvent (75% v/v glycerol–water) to internal ligand binding in myoglobin. When the solvent relaxation is slow compared to intramolecular events we observe decoupling of protein motions from the solvent. In the opposite limit there is a significant contribution of the solvent to internal friction. The solvent enhances the apparent activation energy of transitions in myoglobin. This result is discussed in terms of a generalized Kramers' law involving a dynamic friction coefficient.

Keywords: Specific heat spectroscopy; Flash photolysis; Solvent damping; Myoglobin; Dynamic friction coefficient

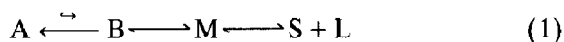
1. Introduction

The high resolution X-ray structures of ligated and unligated myoglobin do not reveal any pathway connecting the heme pocket to the solvent [1]. Thus structural fluctuations, which create transient channels, must play a crucial role in the binding of ligands to the heme iron. The kinetics of ligand binding can be studied with high precision over a large range of temperatures and time scales using flash photolysis [2]. For these reasons mainly, myoglobin has become a model system for studying the relation of motion to function in proteins. In particular, if the motion of the gate

controlling the access of ligands to the heme pocket couples to collective fluctuations, one expects intramolecular processes to depend on the dynamic properties of the solvent. This aspect raises some basic questions which concern the degree of damping of internal protein reactions. In the widely used transition state theory one implicitly assumes intermediate damping and static barriers. The resulting transition rates are independent of friction. Strong damping would lead to Kramers' law of escape rates [3] which is inversely proportional to the friction coefficient f , evaluated near the top of the barrier. If the barrier fluctuates as a result of collective protein motion, which displaces solvent molecules, one expects f to depend on the viscosity η of the solvent. Exactly this result was obtained in flash photolysis experiments on myoglobin using glycerol–water solvents of various composition [4].

¹ Present address: University of Florida, Orlando, FL, USA.
Correspondence to: Dr. W. Doster, Technische Universität München, Physik-Department E13, D-8046 Garching (FRG)

The kinetics of ligand recombination to myoglobin may be approximated by a sequential scheme [5]:



where A refers to the ground state with the ligand (O₂ or CO) attached to the heme iron. B corresponds to the geminate pair after photolysis with the ligand confined to the heme pocket. Below about 160 K only the direct process B → A is observed. At higher temperatures rebinding slows down. Initially, this effect was interpreted as the ligand entering the protein matrix before rebinding which involves the new state M. More recently evidence is mounting that B → M is caused as least in part by relaxation of the heme during rebinding [6,7]. Above 220 K a significant fraction of ligands escapes to the solvent, this state is denoted by S + L. For myoglobin it was found that the solvent composition affects all steps significantly [4,8]. However, assuming Kramers' law, it was found that the friction coefficient would vary sublinearly with the solvent viscosity $f \sim \eta^\kappa$, $\kappa < 1$ [4]. Furthermore, above a critical viscosity η_c , f became independent of the solvent composition. In a theoretical analysis of these data, it was proposed [9] that the effective friction may result not only from fast collisions ($\approx 10^{13} \text{ s}^{-1}$) but includes a second contribution from slow structural fluctuations which modulate the barrier. In that case the static friction has to be replaced by a dynamic one, and f is evaluated at frequencies which correspond to the inverse lifetime λ_r near the top of the barrier. It follows immediately that, if the solvent relaxation rate k_s becomes less than λ_r , one should observe a cross-over to a viscosity independent regime. To evaluate $f(\lambda_r)$ one has to know the entire spectrum of structural fluctuations $f(z)$. Assuming a spectrum which contains two components, solvent dependent and solvent independent protein modes, the sublinear dependence of the friction on viscosity could be explained [9]. The solvent dependent relaxation rates vary in proportion to $k_s \sim \eta^{-1}$. Thus, a knowledge of k_s and not just the viscosity of the solvent is required for a quantitative analysis. We have measured k_s using spe-

cific heat spectroscopy, a new technique [10,11] which we describe in detail below. Since there may be changes unrelated to viscosity at variable solvent composition, we exploit that glycerol-water solvents are excellent glass formers whose viscosities vary by many decades in the vicinity of the glass transition.

In the following we first describe the technique of specific heat spectroscopy and present relaxation measurements carried out using 75% (v/v) glycerol-water mixtures with and without myoglobin. Besides the average relaxation rate k_s we obtain the distribution of relaxation times. For the same system and the same temperature range we display flash photolysis experiments, which allows us to extract the rates k_{BA} , k_{BM} , and k_{MA} of eq. (1). The temperature dependence of these internal rates is then compared to k_s and the conclusions derived from variable solvent experiments are reexamined.

2. Specific heat spectroscopy

2.1 Theory

Calorimetry allows to study the energetics of structural transitions in biomolecules. In the most common method, differential scanning calorimetry, the temperature of the sample is changed over time (t) at constant rate \dot{T} (i.e. dT/dt) while the required power \dot{Q} is recorded. This experiment measures the specific heat of the sample:

$$\dot{Q} = c_p \dot{T}. \quad (1)$$

In many cases c_p is time independent and the experiment provides the true thermodynamic specific heat. However, structural transitions such as unfolding or folding of proteins involve slowly relaxing degrees of freedom. Thus, if the scanning rate is too fast, the system no longer adjusts to the temperature change adiabatically and the specific heat becomes time dependent. This non-stationary specific heat describes the enthalpy relaxation of the system and contains information on the mechanism of structural transitions and

intermediate states. Slow relaxation processes in liquids have been studied by specific heat spectroscopy, a new method proposed by Birge and Nagel [10]. An alternating current is passed through a thin nickel film which was evaporated onto a glass substrate. The film heats the sample at a defined frequency and serves at the same time as a thermometer recording the temperature oscillations at the film-sample interface. This technique allows to derive the product of thermal conductivity and a frequency dependent specific heat $c_p(\omega)$, which characterises the enthalpy relaxation of the liquid. Consider for example a temperature-jump experiment, where one instantaneously raises the temperature at the surface of a thin sample. The time evolution of the adsorbed heat shows a fast initial response due to thermalisation of vibrational degrees of freedom which is followed by a slow component reflecting structural relaxations in the system. This can be written mathematically as the product of a temperature step ΔT at $t = 0$ and a time dependent specific heat:

$$\Delta Q(t) = \Delta T [c_{p,\infty} + (c_{p,0} - c_{p,\infty})(1 - \phi(t))], \quad (2)$$

where $c_{p,\infty}$ denotes the “infinitely” fast phonon component and $\phi(t)$ the normalised response function of the slow part, i.e. $\phi(0) = 1$, $\phi(t \rightarrow \infty) = 0$.

The system thus has a “memory”, which means that for calculating the heat absorbed at a certain time t , one has to sum up over all temperature variations that have occurred at past times $t' < t$. Mathematically this is described by the following convolution integral:

$$\Delta Q(t) = \int_{-\infty}^t dt' c_p(t-t') \Delta \dot{T}(t'). \quad (3)$$

There are generally two ways to determine the relaxation properties of a system: either by directly measuring the time dependent answer to steplike external forces or equivalently by monitoring the extent to which a monochromatically oscillating disturbance is absorbed—a so-called spectroscopic measurement. The two are mathe-

matically connected by a Fourier–Laplace transform. Fourier transformation of eq. (3) yields:

$$\Delta Q(\omega) = c_p(\omega) \Delta T(\omega), \quad (4)$$

with

$$c_p(\omega) = c_{p,\infty} + (c_{p,0} - c_{p,\infty}) \int_0^{\infty} dt e^{i\omega t} [-\dot{\phi}(t)]. \quad (5)$$

It has to be emphasized that these linear response relations are only valid for very small external forces, otherwise higher order corrections would have to be considered. Equation (5) shows that the existence of slow processes, i.e. $\Delta c_p = c_{p,0} - c_{p,\infty} \neq 0$, leads to a complex specific heat, which in turn becomes manifest as a phase-shift between temperature and heat oscillations. The most simple form of a relaxation function is the exponential function which yields as susceptibility the so-called Debye function. Cole and Davidson introduced a modified form (CD distribution) to account for the non-exponential relaxation observed in supercooled liquids and polymers:

$$c_p(\omega) = c_{p,\infty} + \Delta c_p \left(\frac{1}{1 - i\omega\tau} \right)^\beta, \quad \beta \leq 1, \quad (6)$$

which contains the Debye case for $\beta = 1$. In evaluating experimental data, we use a form normalised to the static, i.e. zero-frequency specific heat $c_{p,0}$:

$$\frac{c_p(\omega)}{c_{p,0}} = \gamma + (1 - \gamma) \left(\frac{1}{1 + i\omega\tau} \right)^\beta, \quad (7)$$

where $1 - \gamma = 1 - c_{p,\infty}/c_{p,0}$ is the relative drop of susceptibility across the dispersion region.

Below we discuss the average relaxation rate k_s which for a CD distribution is given by $k_s = (\beta\tau)^{-1}$. Aside from the nonexponential shape of the relaxation function $\phi(t)$, the relaxation rate k_s generally shows a non-Arrhenius temperature dependence in supercooled liquids. Several empirical equations have been proposed to describe the data. In this work we use a formula derived

by Bässler [12] because it contains only two parameters:

$$k_s = k_0 e^{-(T_0/T)^2}, \quad (8)$$

2.2 Technique

In specific heat spectroscopy a thin rectangular nickel film ($d \gtrsim 400 \text{ \AA}$) is evaporated onto a substrate of window glass and is immersed into the liquid to be examined. When a sinusoidal current is passed through it, $I(t) = I_0 \cos \frac{1}{2} \omega t$, a Joulean heat proportional to the square of the current is produced, which has a component constant in time and one that oscillates with frequency ω :

$$Q(t) = \frac{1}{2} R I_0^2 (1 + \cos \omega t). \quad (9)$$

This heat flows into both the window glass substrate and the sample. While the constant source leads to a static temperature gradient across the two bulks, the harmonic one creates an exponentially damped temperature wave in each of them (real part solution). This result is obtained by solving the one-dimensional heat diffusion equation with the heat source at $x = 0$ and the glass substrate (index 1) and sample (index 2) at $x < 0$ and $x > 0$, respectively:

$$\Delta T(x, t) = \mathcal{R}\{\Delta T_{x=0} e^{i(\omega t - \pi/4)} e^{k_j x}\}, \quad (10a)$$

with

$$k_j = \pm(1+i) \sqrt{\frac{\omega c_{pj} \rho_j}{2\kappa_j}}, \quad j = 1, 2. \quad (10b)$$

Here ρ_j , c_{pj} and κ_j denote the mass density, the specific heat and the thermal conductivity, respectively. The wavelength of the thermal wave is given by $\lambda_j = 1/k_j$ and varies as $1/\sqrt{\omega}$. The one dimensional treatment of the problem is justified, if this wavelength is considerably smaller than the lateral dimensions of the film.

For the temperature oscillation at the nickel film, i.e. $x = 0$, one obtains:

$$\Delta T_{x=0,t} = \frac{Q_0}{\sqrt{\omega} (\sqrt{\epsilon_1} + \sqrt{\epsilon_2})} \frac{1}{2} \cos(\omega t - \frac{1}{4}\pi), \quad (11)$$

where $\epsilon_j = c_{pj} \rho_j \kappa_j$ is the so-called thermal effusivity and $Q_0 = R I_0^2$ the amplitude of the oscillating heat source. The experiment thus yields the product of specific heat and thermal conductivity. The heat source can serve at the same time as a thermometer since the resistance of the Ni-film depends on temperature according to $R = R_0(1 + \alpha T)$. The temperature oscillations thus induce a time dependent component in the resistance:

$$\Delta R(t) = \alpha R_0 \Delta T_{x=0,t}. \quad (12)$$

According the Ohms law the initial current experiences an additional voltage drop across this oscillating resistance. Mixing of these two oscillations $\frac{1}{2}\omega$ and ω yields a further component of frequency $\frac{1}{2}\omega$ and in addition one of frequency $\frac{3}{2}\omega$. The amplitude of the latter contains information on the heat diffusion properties of the substrate and the sample (eqs. 11, 12):

$$\Delta U_{\frac{3}{2}\omega}(t) = \frac{\alpha R_0 Q_0 I_0}{\sqrt{\omega} (\sqrt{\epsilon_1} + \sqrt{\epsilon_2})} \frac{1}{4} \cos(\frac{3}{2}\omega t - \frac{1}{4}\pi). \quad (13)$$

If the specific heat of a sample becomes complex and frequency dependent — as is the case for a supercooled liquid in the dispersion region — a phase-shift in addition to the intrinsic $\frac{1}{4}\pi$ between the heat source and the temperature response occurs, as well as an additional frequency dependence of the amplitude via $\epsilon_2 = \epsilon_2(\omega)$. Thus a measurement of the amplitude and the phase shift of the $\frac{3}{2}\omega$ -component by means of a lock-in amplifier yields modulus and phase and therefore the real and imaginary part of the specific heat.

The signal amplitude $\Delta U_{\frac{3}{2}\omega}$ is superimposed onto the initial voltage drop $\dot{U}(t) = R_0 I(t)$ across the film, but is smaller by approximately four orders of magnitude. Thus $\Delta U_{\frac{3}{2}\omega}$ cannot be measured directly by a lock-in amplifier, because the latter component would overload the input preamplifier. Therefore the film is inserted into one arm of a Wheatstone bridge, which is balanced with respect to the large $\frac{1}{2}\omega$ component and thus allows the $\frac{3}{2}\omega$ amplitude to be measured across the bridge. Figure 1 shows the experimental setup. We have performed measurements of

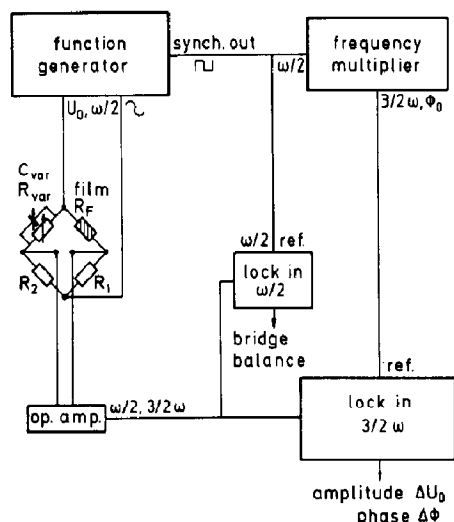


Fig. 1. Experimental setup of the specific heat spectrometer: Film: 500 Å Ni on a glass substrate (1 × 2 cm), the frequency multiplier is home-made and consists of a phase-locked loop which provides a stable reference phase ϕ_0 . One lock-in amplifier is used to minimize the $\frac{1}{2}\omega$ component by varying R_{var} , C_{var} . The second lock-in determines amplitude and phase shift of the $\frac{3}{2}\omega$ signal. Bridge parameters: $R_F \approx 15 \Omega$, $R_1 = 35 \Omega$, R_{var} , $R_2 \approx 2 \Omega$. The operational amplifier decouples the frequency generator from the lock-in to avoid ground loops. The $\frac{3}{2}\omega$ signal varies by 10 μV across the glass transition.

the frequency dependent specific heat on a 10 mM solution of horse myoglobin in a 75% (v/v) mixture of glycerol–water and of the solvent alone.

2.3 Results

The glass transition of a 75% (v/v) glycerol–water mixture determined from the step in the specific heat in a scanning calorimetry experiment (20 K/min) occurs at 175 K. The modulus in the dynamic experiment $\epsilon \sim c_p$ shows the same behaviour (Fig. 2), however, the transition temperature increases with frequency. This is the signature of a time or frequency dependent specific heat as a result of slowly relaxing degrees of freedom. Moreover, the phase lag of the temperature oscillations with respect to the heat oscillations shows a maximum at the midpoint of the transition. At the maximum one has $\omega\tau \approx 1$, $\tau = 1/k_s$ and this allows to derive the temperature

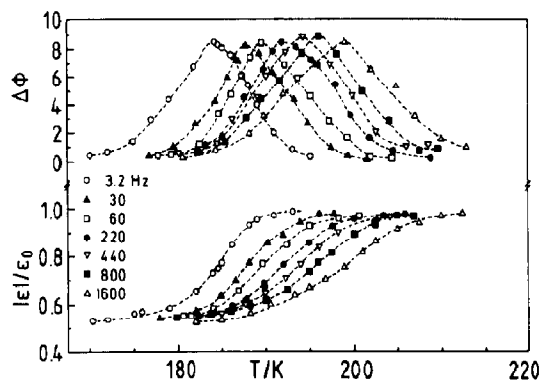


Fig. 2. Normalized effusivity and phase-shift of a 75% (v/v) glycerol–water mixture at various experimental frequencies $\omega/2\pi$.

dependence of k_s as shown in Fig. 4. Furthermore, the shape of the transition curves is not compatible with a single relaxation process but a Cole–Davidson function (eq. 7) can approximately account for the data. The same experiment was performed using a myoglobin solution (10 mM) and typical results are shown in Fig. 3 together with fits to a Cole–Davidson function. The average relaxation times of solvent and solution are quite similar (Fig. 4 and Table 1). The

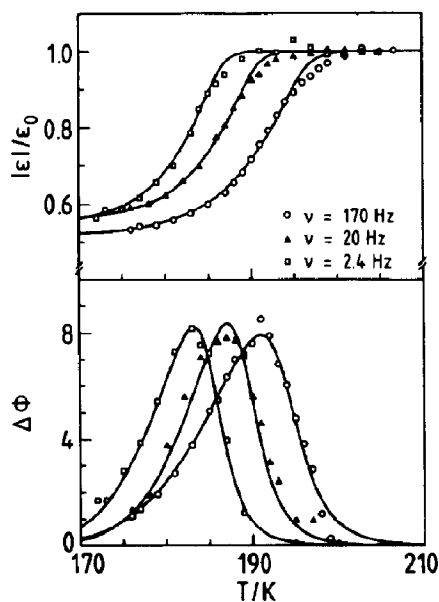


Fig. 3. Normalized effusivity and phase-shift of a 10 mM myoglobin solution together with fits to a Cole–Davidson distribution. Parameters are given in Table 1.

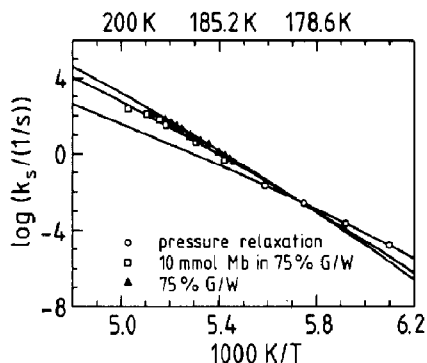


Fig. 4. Arrhenius plot of the average relaxation rates k_s (\square , \blacktriangle) and pressure relaxation data (\circ) as described in the text. The lines are fits to eq. (8), the parameters are given in Table 1.

protein, however, broadens the transition, decreasing β . It is plausible that the protein has only a tiny effect on the average relaxation rate k_s since the intrinsic viscosity of the molecule is small compared to the bulk viscosity of the glycerol–water solvent. But the broadening of the relaxation time spectrum shows that the protein has a profound effect on the enthalpy relaxation of the solution. In Fig. 5 we display the resonance peak versus $\omega\tau$ on a logarithmic scale covering eight orders of magnitude, which should map the data obtained at various frequencies on one curve. This procedure works very well for the solvent but fails in the case of the solution at high frequencies. The solution shows a strongly stretched high frequency part which itself depends on frequency. The variation is non-monotonic reaching a maximum near 380 Hz. A plausible explanation could be a weakly temperature dependent protein mode which is excited near 380 Hz. In the

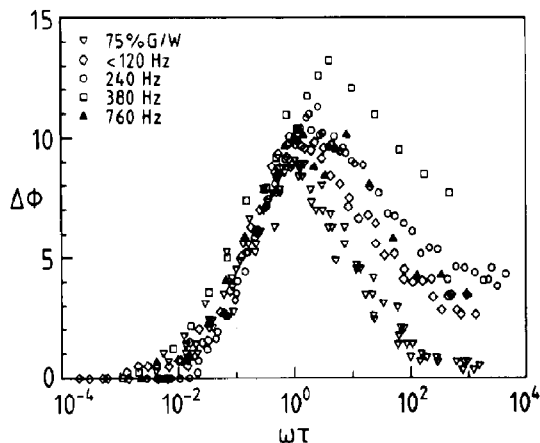


Fig. 5. Phase shift versus $\omega\tau$: The inverted triangles (∇) combine all experiments performed with the solvent. The other symbols refer to the protein solution.

following we confine the discussion to the average rate k_s .

3. Flash photolysis

3.1 Method

The kinetics of recombination of horse myoglobin (Sigma) and carbon monoxide was studied by laser photolysis [2]. The protein was dissolved in 75% (v/v) glycerol–water mixtures (pH 7) equilibrated at 1 atm CO pressure and was reduced by a ten-fold excess of dithionite. The solution (4 mM) was filled into a thin optical cell (spacing 15 μm) which was attached to a helium flow cryostat. Photolysis was achieved using the 8 ns pulse (120 mJ) of a frequency doubled Nd-YAG laser (Spectra Physics) at 532 nm. The

Table 1

Average solvents and solution specific heat parameters (CD-fits in Fig. 3)

Solvent	$\log k_0$	T_0	β_{CD}	γ
Glycerol [10]	20.16 ± 0.5	1358 ± 6	0.44 ± 0.03	0.52 ± 0.03
75% (v/v) glycerol–water	20.8	1236	0.48 ± 0.03	0.47 ± 0.03
10 mM horse myoglobin	22.4	1288	0.31 ± 0.02	0.54 ± 0.03
75% (v/v) glycerol–water				
Pressure relaxation [15]	14.7	1092	0.47	

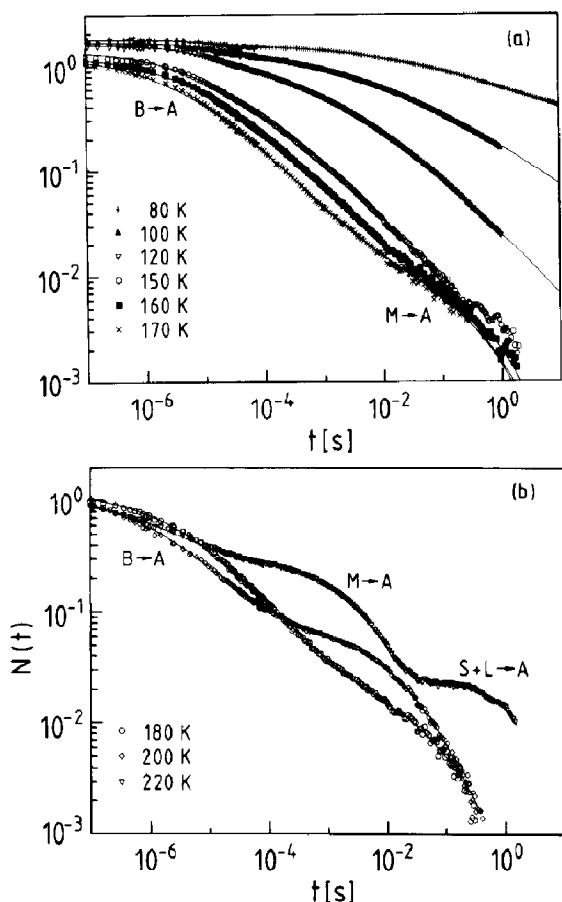


Fig. 6. Survival fraction of photolyzed protein $N(t)$ showing the three relevant processes $B \rightarrow A$, $M \rightarrow A$, $S + L \rightarrow A$ below (a) and above (b) the glass transition temperature (175 K).

transient optical absorption at 436 nm was recorded using a home-made, microprocessor-controlled log-time averager covering a time range between 10^{-6} and 10^2 s and about three decades in extinction, and a fast digital oscilloscope (Gould) for times between 10^{-7} and 10^{-5} s.

3.2 Results and data analysis

In Fig. 6 we show some representative results of the flash photolysis experiment. Three processes $B \rightarrow A$, $M \rightarrow A$ and at higher temperatures $S + L \rightarrow A$ can be identified. The survival fraction of deligated molecules $N(t)$ is thus written

as a sum of three components according to the sequential scheme of eq. (1):

$$N(t) = N_{BA}(t) + N_{MA}(t) + N_s(t) \quad (12)$$

The strongly non-exponential process $B \rightarrow A$ is analyzed in terms of a temperature invariant distribution of activation energies $g(H_{BA})$

$$N_{BA}(t) = N_{BA}^0 \int_0^\infty g(H_{BA}) e^{-k(H_{BA})t} dH_{BA} \quad (13)$$

assuming the Arrhenius law: $k = A e^{-H_{BA}/RT}$. For $g(H_{BA})$ we use the Gamma distribution as proposed by Young and Bowne [14]. The essential parameters are $A = 2 \cdot 10^9 \text{ s}^{-1}$ and $H_{BA} = 11.5 \text{ kJ/mol}$. Process $M \rightarrow A$ is approximated by a stretched exponential:

$$N_{MA} = N_M^0 e^{-(t/\tau)^\beta} \quad (14)$$

which allows us to determine the average rate as $k_{MA} = \beta/\tau \Gamma(1/\beta)$, where $\Gamma(x)$ is the Gamma function. $S + L \rightarrow A$ is described by bimolecular kinetics. The extraction of k_{BM} is more complex. The amplitude N_M^0 in a sequential model (eq. 1) is given by:

$$N_s^0 + N_M^0 = \left\langle \frac{1}{1 + k_{BA}(H_{BA})/k_{BM}} \right\rangle_{H_{BA}} \quad (15)$$

which has to be averaged with respect to the distribution of H_{BA} . We first determine N_M^0 by fitting the data to eqs. (12–14). We multiply however, $N_{BA}(t)$ by a cut-off function $\exp(-t/\tau_c)^\beta$ to account for the missing contribution which is converted from B to M . k_{BM} is then determined iteratively using eq. (15) and the unperturbed $g(H_{BA})$: k_{BM} is varied until the right hand side of eq. (15) agrees with the experimental N_M^0 . We note that the choice of $\langle \tau_c \rangle^{-1}$ has about the same magnitude and temperature dependence as k_{BM} . Judging from the variance of the parameters (see multiple points in Fig. 7) we determine k_{BM} within a factor of two. This analysis assumes exponential kinetics of $B \rightarrow M$ which may be an approximation. We have checked that one determines with this procedure the average rate unless the distribution of rates is highly exotic.

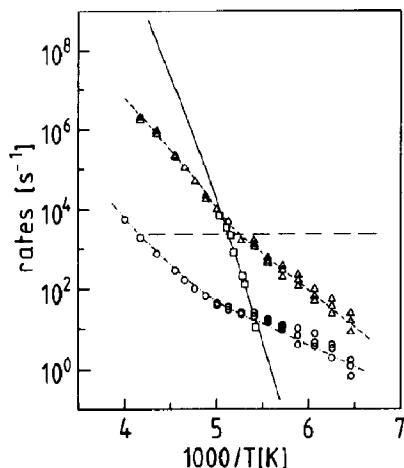


Fig. 7. Arrhenius plot of solvent and protein relaxation rates: (\square) k_s of the protein solution, (Δ) k_{BM} , and (\circ) k_{MA} . Solid line: fit of k_s to eq. (8). Dotted line: fit of k_{BM} to the dynamic friction model $\kappa = 0.2$. Dashed line: frequency (380 Hz) where the anomaly in $c_p(\omega)$ of the protein solution is observed. Dashed-dotted line: fit of eqs. (18, 21, 22) to k_{MA} .

Figure 7 shows an Arrhenius plot of the resulting k_{BM} , k_{MA} together with k_s derived from the specific heat experiment. At first sight there seems to be little correlation between the three data sets, at least there is no parallel freezing-in of solvent and protein motions. However, the slope of $k_{BM}(T)$ shows a discontinuity at the temperature where the solvent relaxation rate crosses k_{BM} . The apparent activation energy decreases by about 20 kJ (51 to 32 kJ/mol) which is just the opposite expected for parallel freezing in. It seems more likely that the protein transition decouples from the solvent for k_s less than k_{BM} . The same decoupling effect is observed, even more pronounced, for k_{MA} at about the same temperature. A similar result has been obtained before in the variable solvent experiment at constant temperature: The transition rates became independent of the solvent above a critical viscosity η_c [4]. The dashed line corresponds to a frequency of 380 Hz where the anomaly in the specific heat experiment was observed. It is very close to the cross-over rate of solvent and protein relaxation supporting the tentative explanation given above.

Finally, in Fig. 4 we compare pressure jump induced structural relaxation, where the CO

stretching vibration of MbCO is used as a monitor to solvent relaxation rates [15]. The relaxation time distribution of the conformational change is much wider as compared to the solvent. We parametrized the initial phase of the pressure release kinetics using a stretched exponential with $\beta = 0.6$. The resulting average relaxation rate is shown in Fig. 4. The pressure relaxation data seem to have a slightly weaker temperature dependence than the solvent suggesting again decoupling. But given the uncertainties of the extrapolation one cannot exclude that this process freezes in parallel with the solvent.

5. Discussion: A dynamic friction model

Our experiments suggest that solvent relaxation affects internal processes in myoglobin. The correlation is more subtle than expected for a "slaved" motion. Our data are consistent, however, with results obtained at variable solvent composition: The internal rates decouple from the solvent rather than being slaved above a critical viscosity. The experimental evidence is the discontinuity in the apparent activation energy at a temperature where the relaxation time of the solvent crosses the characteristic time of the process. This temperature is about 200 K, far above the glass temperature of the solvent of 175 K, suggesting a dynamic mechanism.

In the following we connect these experiments with a mechanism of solvent damping which relies on the concept of a dynamic friction $f(z)$ [9], which is defined by:

$$f(z) = \int_0^{\infty} e^{-zt} f(t) dt \quad (16)$$

where $f(t)$ is proportional to the random force autocorrelation function of the heat bath. If the fluctuations of the heat bath are fast compared to the time scale of the relevant process one can use the static friction $f_{z=0}$. We are, however, concerned with barrier-fluctuations in the protein which do not necessarily meet this requirement. In ref. [9] it was proposed to relate $f(t)$ to the density correlation function $\phi(t)$ of the protein

structure, $f(t) \sim F(\phi(t))$ which was approximated by:

$$f(t) \sim (k_p t)^{\kappa-1} e^{-k_s t}, \quad \kappa \leq 1, \quad t \gg \tau_p^{-1} \quad (17)$$

The power law describes a broad spectrum of local, solvent independent modes and the exponential approximates collective, solvent-coupled fluctuations. In eq. (17) k_p denotes the relaxation rate of solvent decoupled motions and $k_s \sim 1/\eta$ is the rate of solvent-controlled structural fluctuations. Thus k_p and κ do not depend on k_s . Recent inelastic neutron scattering experiments on myoglobin [16], which measure $\phi(t)$, confirm the general structure of eq. (17). A mode coupling analysis of these data suggests [17]: $f(t) = A\phi(t) + B\phi(t)^2$. A detailed discussion is presented elsewhere. Here, we rely on eq. (17) and obtain (cf. eq. 16) [9]:

$$f(z) = \frac{k_0^2}{k_p} \left(\frac{z + k_s}{k_p} \right)^{-\kappa} \quad (18)$$

k_0 is the decay rate of the velocity autocorrelation function due to fast collisions, typically 10^{13} s^{-1} . We now consider the relaxation of a particle in a harmonic potential assuming strong damping. The rate is given by

$$k = \omega_0^2 / f_{z=k} \quad (19)$$

The friction has to be evaluated at $z = k$, which denotes the relevant time scale of the process. From eqs. (18) and (19) we obtain the implicit equation:

$$k = \frac{\omega_0^2 k_p}{k_0^2} \left(\frac{k + k_s}{k_p} \right)^{\kappa} \quad (20)$$

Thus, for $k \ll k_s$, k varies in proportion to $k_s^{\kappa} \sim \eta^{-\kappa}$ which gives Stokes' law, $k \sim 1/\eta$, for $\kappa = 1$. If $k \gg k_s$, k becomes independent of k_s , the transition occurs at $k = k_s$. In Fig. 7 we observe a discontinuity in the temperature dependence of k_{BM} at $k_{\text{BM}} \approx k_s$. This result can be explained by eq. (20), assuming that $B \rightarrow M$ corresponds to overdamped relaxation in a harmonic potential. The fit to the data gives $\kappa = 0.2$. Note that $B \rightarrow M$

involves the relaxation of the protein towards the deoxy structure, k_{BM} is close to the relaxation rate κ^* of ref. [6] obtained for sperm whale myoglobin. Photolysis thus generates an unstable state B which relaxes towards a minimum M in the potential energy hypersurface.

For a process controlled by a barrier, Grote and Hynes [18] derived a generalized Kramers' law of escape rates covering intermediate and strong damping:

$$k = k^{\text{TST}} \lambda_r / \omega_r \quad (21)$$

k^{TST} is the transition state result, $k^{\text{TST}} = \omega_0 e^{-H/RT}$, ω_r denotes the frequency of the inverted harmonic potential at the top of the barrier. λ_r denotes the rate of the unstable motion on the barrier:

$$\lambda_r = \omega_r^2 / (\lambda_r + f(\lambda_r)) \quad (22)$$

Equations (21) and (22) collapse to the transition state result for $\lambda_r \gg f(\lambda_r)$ or intermediate damping. We are interested in the Kramers' limit, $\lambda_r \ll f(\lambda_r)$, of strong damping. The dynamic friction has to be evaluated near λ_r (not k) because λ_r is now the relevant time scale for damping near the top of the barrier. Since the cross-over in the temperature dependence of k_{MA} occurs approximately at the temperature where $k_s = k_{\text{BM}}$ but $k_{\text{MA}} \ll k_s$, we conclude that $M \rightarrow A$ is controlled by a barrier. The transition is thus determined by the condition $\lambda_r^c = k_s$. Using again the dynamic friction model of eq. (17) and solving eq. (21) and (22) numerically we obtain a reasonable fit to the data (Fig. 7). The parameters are: $\kappa = 0.3$, $\lambda_r^c = 2 \cdot 10^5 \text{ s}^{-1}$, $H_{\text{MA}} = 19 \text{ kJ/mol}$. The last number is in agreement with results of Ref. [6], where this barrier is assumed to control CO binding in the relaxed (deoxy) structure. Taking $k_0 \approx 10^{13} \text{ s}^{-1}$ and $k_p \approx 10^{11} \text{ s}^{-1}$ (β -relaxation) as suggested by inelastic neutron scattering experiments [16] one obtains an estimate of $\omega_r \approx 10^{11} \text{ s}^{-1}$ and $\omega_0 = 10^{12} \text{ s}^{-1}$. The dynamic friction concept thus provides a framework to understand solvent damping on internal protein motions. All parameters have a well-defined physical meaning. The description is simplified because it is one-dimensional, friction anisotropy effects are ignored [19].

Related generalizations of Kramers' theory have been published [20–23].

We conclude that the solvent can enhance the apparent activation energy of internal protein processes via friction. For aqueous solutions and physiological temperatures the solvent friction may contribute up to 10 kJ/mol (assuming $\kappa = 0.5$), since water has an apparent activation energy of 20 kJ/mol [24]. To obtain these results it was essential to rely on specific heat spectroscopy. This technique could in principle be applied to other dynamic biological phenomena in the Hz to kHz range. Sensitivity considerations suggest that the specific heat of the system should change roughly by a factor of two. This may require significant solute concentrations. The solvent viscosity dependence of protein internal motions has been analysed by a generalized Kramer's equation involving a variety of systems [25–29]. This question also gains relevance in the context of computer simulations of hydrated proteins [30,31].

Acknowledgements

We thank S. Nagel, H. Frauenfelder, B. Büchner, P. Korpiun, and the late Edgar Lüscher for the stimulating discussions and H. Hagn for the excellent technical support. The work is supported by a grant of the Deutsche Forschungsgemeinschaft.

References

- 1 T. Tanako, *J. Mol. Biol.* 110 (1977) 537.
- 2 R.H. Austin, K.W. Beeson, H. Frauenfelder and I. Gunsalus, *Biochem.* 14 (1975) 5355.
- 3 H.A. Kramers, *Physica* 7 (1940) 284.
- 4 D. Beece, L. Eisenstein, H. Frauenfelder, M. Marden, L. Reinisch and K.T. Yue, *Biochem.* 19 (1980) 5147.
- 5 W. Doster, D. Beece, S.F. Di Iorio, L. Eisenstein, H. Frauenfelder, L. Reinisch, E. Shyamsunder, K. Winterhalter and K. Yue, *Biochem.* 21 (1982) 4831.
- 6 P.J. Steinbach, A. Ansary, J. Berendzen, D. Braunstein, K. Chu, B.R. Cowen D. Ehrenstein, H. Frauenfelder, J.B. Johnson, D.C. Lamb, S. Luck, J.R. Mourant, G.U. Nienhaus, P. Ormos, R. Philipp, A. Xie and R.D. Young, *Biochem.* 30 (1991) 3988.
- 7 M.K. Hong, E. Shyamsunder, R.A. Austin, B.S. Gerstman and S.S. Chan, *Phys. Rev. Lett.* 66 (1991) 2673.
- 8 E. DiIorio, U.R. Hiltbold, D. Filipovic, K.H. Winterhalter, E. Gratton, E. Vitrano, A. Cupane, M. Leone and L. Cordone, *Biophys. J.* 59 (1991) 742.
- 9 W. Doster, *Biophys. Chem.* 17 (1983) 97.
- 10 N.O. Birge and S.R. Nagel, *Phys. Rev. Lett.* 54 (1985) 2674.
- 11 B. Büchner and P. Korpiun, *Appl. Phys.* B43, (1987) 29.
- 12 H. Bässler, *Phys. Rev. Lett.* 58 (1987) 767.
- 13 N.O. Birge and S. Nagel, *Rev. Sci. Instrum.* 58 (1987) 1464.
- 14 D. Young, S. Bowne, *J. Chem. Phys.* 81 (1984) 3730.
- 15 I.E. Iben, D. Braunstein, W. Doster, H. Frauenfelder, M.K. Hong, J.B. Johnson, S. Luck, P. Ormos, A. Schulte, P.J. Steinbach, A.H. Xie and R.D. Young, *Phys. Rev. Lett.* 62 (1989) 1916.
- 16 W. Doster, S. Cusack and W. Petry, *Nature (London)* 337 (1989) 754.
- 17 W. Doster, S. Cusack and W. Petry, *Phys. Rev. Lett.* 65 (1990) 1080.
- 18 R.F. Grote, J.T. Hynes, *J. Chem. Phys.* 74 (1981) 4965.
- 19 A.M. Berezhkovskii, L.M. Berezhkovskii and V. Zitserman, *Chem. Phys.* 130 (1989) 55.
- 20 Y.A. McCammon and P. Wolynes, *J. Chem. Phys.* 66 (1977) 1452.
- 21 B. Gavish, *Phys. Lett.* 44 (1980) 1160.
- 22 P. Hänggi, P. Talkner and M. Borkovec, *Rev. Mod. Phys.* 62 (1990) 251.
- 23 J. Schlitter, *J. Chem. Phys.* 120 (1988) 187.
- 24 G.P. Singh, F. Parak, S. Hunklinger and K. Dransfeld, *Phys. Rev. Lett.* 47 (1981) 685.
- 25 A. Rosenberg, K. Ng and M. Punyiczki, *J. Mol. Liq.* 42 (1989) 31.
- 26 K. Ng and A. Rosenberg, *Biophys. Chem.* 39 (1991) 57.
- 27 H.J. Steinhoff, *Eur. Biophys. J.* 18 (1990) 57.
- 28 E.W. Findson, J.M. Friedman and M.R. Ondrias, *Biochem.* 27 (1988) 8719.
- 29 D. Beece, S.F. Brown, J. Czege, L. Eisenstein, H. Frauenfelder, D. Good, M.C. Marden, J. Marque, P. Ormos, L. Reinisch and K.T. Yue, *Photochem. Photobiol.* 33 (1981) 517.
- 30 J. Smith, K. Kuczera and M. Karplus, *J. Mol. Biol.* 215 (1990) 439.
- 31 R.J. Loncharich and B.R. Brooks, *J. Mol. Biol.* 215 (1990) 439.